10th International Conference on Fracture Mechanics of Concrete and Concrete Structures
FraMCoS-X
G. Pijaudier-Cabot, P. Grassl and C. La Borderie (Eds)
https://doi.org/10.21012/FC10.235480

ALTERATION OF THE FRACTURE BEHAVIOR IN HOST ROCK DURING CO_2 GEOLOGICAL SEQUESTRATION

ANGE-THERESE AKONO[*], THEODORE T. TSOTSIS[†] AND CHARLES J. WERTH[†]

[*] Northwestern University
2145 Sheridan Road,
Evanston, 60208, 60208, USA
e-mail: ange-therese.akono@northwestern.edu

[†] University of Southern California
925 Bloom Walk,
Los Angeles, CA, 90089, USA
e-mail: tsotsis@usc.edu

[†] University of Texas at Austin
301 E. Dean Keeton., Stop C1786
Austin, TX 78712, USA
e-mail: werth@utexas.edu

Key words: CO_2 Geological Storage, Geochemical Reactions, Scratch Tests, Size Effect Law

Abstract: Our research objective is to understand the evolution of the fracture behavior of host rock during CO_2 sequestration. We focus our study on the Mt. Simon sandstone as part of the Illinois Basin Decatur Project, Illinois, USA. We conduct microscopic scratch tests, ion chromatography tests, environmental back-scattered secondary electron microscopy, and machine learning modelling on both unaltered and altered Mt Simon sandstone. Alteration occurs via incubation in CO_2-saturated brine for seven days at 2500 psi and 50 ℃. The size effect law is applied to extract the fracture parameters from the scratch test measurements. A decrease in fracture toughness and an increase in fracture process zone is observed following incubation of Mt Simon sandstone in CO_2-saturated brine. Furthermore, microstructural changes are observed such as an increase in the overall porosity, an increase in pore throat sizes, and the formation of local porosity gradients. Evidence of K-feldspar dissolution is shown as well. Thus, scratch testing provides a means to quantify the changes in fracture response following potential CO_2-induced geochemical reactions, making the method suitable for quality control and safety design in CO_2 geological sequestration schemes.

1 INTRODUCTION

Geological storage of carbon dioxide (GCS) is a viable alternative that is considered worldwide in other to reduce anthropogenic greenhouse gas emissions. Due to their abundance, saline aquifers represent a preferred option for subsurface storage of carbon dioxide. However, an important question is the impact of CO_2-saturated brine on the mechanical behavior of the host rock. The evolution of the fracture properties in particular is an important question as premature cracking may potentially result in a loss of zonal insulation, fault activation, or microseismicity.

In this study, we investigate the fracture behavior of host rock following incubation with CO_2-saturated brine. Our model material is the Mt Simon sandstone from the Illinois Basin in

Decatur, IL. As part of the US DOE-sponsored Illinois Basin Decatur Project, carbon dioxide was injected into the Mt Simon Sandstone formation at a depth of 7025–7050 ft. (2141.2–2148.8 m) and at a daily rate of 1,000 tons/day from 2011 to 2014 [1]. In parallel, geophones were installed to record microseismic emissions. The subsurface injection of carbon dioxide resulted in a surge of microseismic emissions, with a magnitude less than 2, that continued even after injection had stopped [2]. The reported increase in microseismic emissions following CO_2 injection calls for a deeper investigation into the effect of carbon dioxide and CO_2-induced geochemical reactions on the fracture behavior of host rocks.

We propose a novel approach to investigate alterations in the fracture behaviour of host rocks using nonlinear fracture mechanics integrated with analytical imaging and data science methods. Prior studies have investigated modifications in the fracture behaviour of sandstone following incubation in acidic systems using short rod tests [3,4], double torsion tests, and microscopic scratch tests [5,6]. However, the analysis relied heavily on Linear Elastic Fracture Mechanics models, different geological systems were studied, and relating mechanical changes to microstructural and chemical alterations remained a challenge.

We employ novel fracture testing methods such as scratch testing, nonlinear modeling via the Size Effect Law, and machine learning to probe the behavior of Mt Simon sandstone. This paper is organized as follows. First, we present the experimental methods. Then, we describe the theoretical model for nonlinear fracture assessment via scratch tests and show our results. Finally, we utilize scanning electron microscopy imaging integrated with Gaussian mixture modelling and ion chromatography to investigate CO_2-induced microstructural and chemical changes.

2 MATERIALS AND METHODS

The microstructure, chemistry, and mechanical behavior of Mt Simon sandstone were investigated using scanning electron microscopy, X-ray diffraction analyses, and scratch testing. Mt Simon sandstone cores were provided by the Prairie Institute Geological Core Repository where they had been stored at 4ºC after harvesting. Fig. 1 a) displays a digital photograph of one of our cores, which where extracted from the Mt Simon sandstone formation at a depth of 6925 ft (2110.7 m).

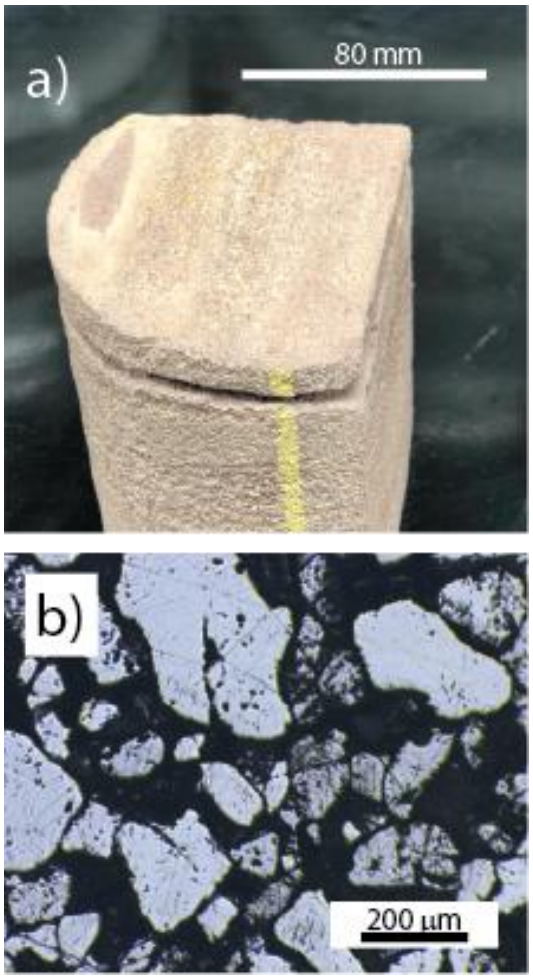

Figure 1: a) Digital photograph of Mt. Simon sandstone core tested in this study. Credit: Ange-Therese Akono, Northwestern University, 2018. B) Optical microscopy image of Mt Simon sandstone specimen after grinding and polishing.

2.1 Specimen Preparation

A rigorous specimen preparation procedure was used to yield specimens with a mirror-like surface and a low surface roughness so as to guarantee the accuracy of the microscopic testing phase. The first step was to cut 1-cm tall rock prisms with a hacksaw at a low speed. The prisms were then cast into epoxy resin. Then, the embedded specimens were machined using

a low-speed diamond saw to yield 4-mm thin slices. The thin slices were mounted on aluminum discs using cyanoacrylate glue and embedded again with a low-viscosity epoxy resin under vacuum so as to fill existing air voids between grains. The double-embedded specimens were ground with an Ecomet 250/Automet® 300 grinder polisher (Buehler, Lakebluff, IL, USA) using silicon carbide grinding pads of increasing grit size. In between each pads, the specimens were rinsed in an ultrasonic bath using N-decane. After grinding, the specimens were polished in two steps. First, hard perforated chemo-textile pads were utilized with a series of diamond slurries of decreasing particle size. Then, fine polishing was carried out using aluminum oxide abrasive discs with decreasing particle size. After grinding and polishing, the Mt Simon sandstone specimens were stored under vacuum pending further testing. Fig. 1 b) displays an optimal microscopy image of a Mt Simon sandstone sample after grinding and polishing, as visualized using a Nikon transmitted light microscope. A porous and granular microstructure is observed with grains ranging from 150–500 μm in size.

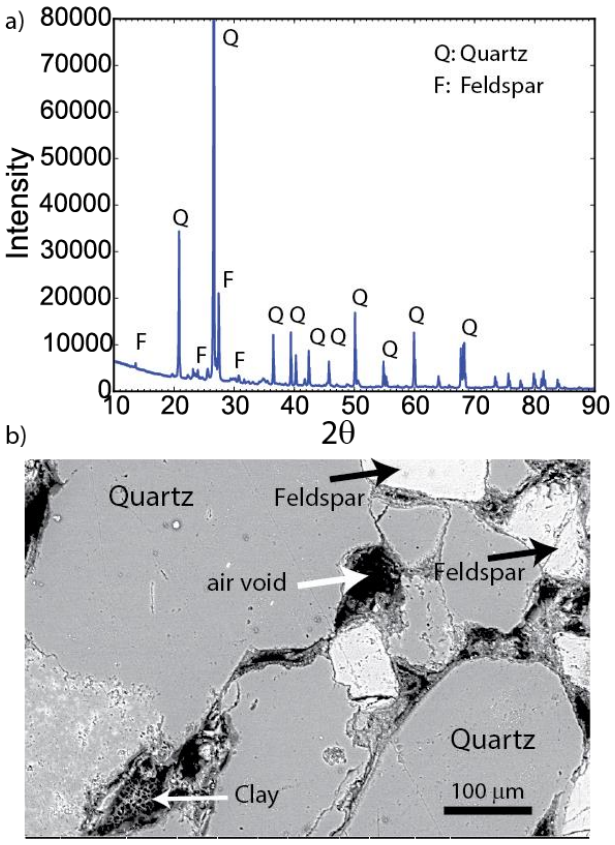

Figure 2: a) X-ray diffractogram of unaltered Mt Simon sandstone sample extracted from depth 6925 ft. b) Environmental back-scattered secondary electron image of unaltered Mt Simon sandstone sample. Quartz grains are in dark gray, whereas feldspar grains are shown in bright color and air voids are shown in black.

2.2 Microstructural and Chemical Characterization

The chemical composition of the Mt Simon sandstone was characterized using powder X-ray diffraction analyses conducted by EAG laboratories (Sunnyvale, CA, USA). Pressed powders of ground rock specimens were analyzed using a Rigaku Smartlab diffractometer. Fig. 2 a) displays the X-ray diffraction spectrum for unaltered Mt Simon sandstone extracted at depth 6925 ft (2110.7 m). The main components are quartz—SiO_2—(66.7% wt) and K-feldspar—$K(Si_3Al)O_8$—(microcline 13.3% wt and sanidine 17.9% wt).

The microstructure was investigated using an environmental scanning electron microscope, FEI Quanta 650, at the Northwestern University Atomic and Nanoscale Characterization center. Backscattered electron imaging was performed under low vacuum using an accelerating voltage of 20 kV, a spot size of 4.2, and with a walking distance of 10.0 mm. Fig. 2 b) displays a characteristic backscattered secondary electron micrograph, showing quartz grains in dark gray, feldspar grains in bright color, and air voids in black. In particular, clay sheet can be observed that surround the grains and serve as cementing agents.

2.3 Incubation in CO_2-Saturated Brine

Mt Simon sandstone samples were incubated using a reactive transport open flow apparatus. A full description of the equipment can be found in [3]. A 1-cm long cubic specimen was aged in CO_2-saturated brine under a pressure of 2500 psi (17.24 MPa) at 50ºC for 7 days. The composition of the synthetic brine is given in Table 1. Before and

after CO_2-incubation, ion chromatography analysis was performed using an ICS-2100 IC system (Dionex) to measure the concentration of cations and anions.

2.4 Scratch Testing

The fracture behavior was characterized using an Anton Paar microscopic scratch tester. In our tests, a spheroconical diamond probe was pushed across the sample at a fixed speed under a linearly increasing vertical force.

Table 1: chemical composition of synthetic brine.

Chemical component	Concentration (g/L)
NaCl	111.67
$CaCl_2 \cdot 2H_2O$	78.35
$MgCl_2 \cdot 6H_2O$	16.53
KBr	6.48
Na_2SO_4	0.48
$SrCl_2 \cdot 6H_2O$	2.37
LiCl	9.36

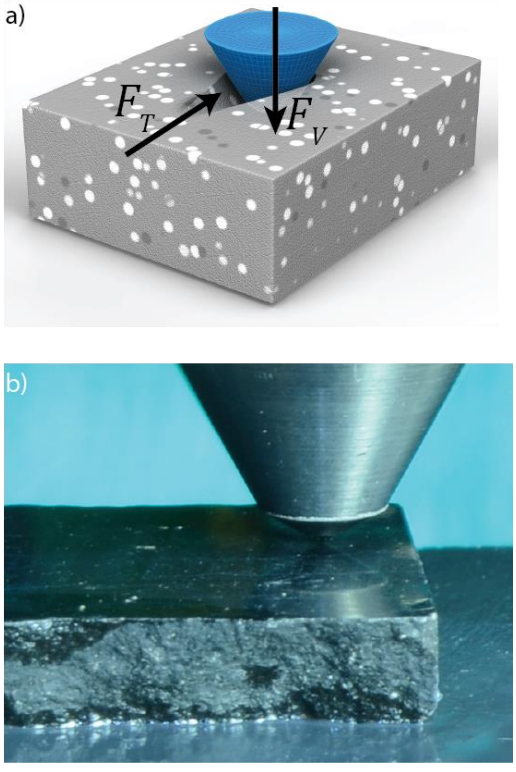

Figure 3: a) Schematic representation of scratch testing. F_V is the prescribed vertical force whereas F_T is the recorded horizontal force. B) Digital photograph of a scratch test on a rock specimen. Credit: Ange-Therese Akono, University of Illinois at Urbana-Champaign, 2014.

Fig. 3 a) illustrates the principle of scratch testing and Fig. 3 b) displays a digital photography of the experimental set-up for a rock specimen. In our tests, a Rockwell C probe was used with a maximum load of 5.5 N, a scratch speed of 6 mm/min, and a scratch length of 3 mm. Prior to testing, the surface roughness was measured using contact profilometry. Using the preparation procedure given in Section 2.1, the average roughness over a length of 3 mm as 0.63 µm.

4 THEORY

We consider a scratch test with a spherical probe of radius R and we seek to relate the measured horizontal force F_T and penetration depth d to the fracture toughness K_c of the material using the Size Effect Law. The starting point is the Linear Elastic Fracture Mechanics (LEFM) solution for scratch testing [7,8]. The LEFM solution was developed assuming brittle fracture, by considering the propagation of a flat semi-circular crack emanating from the tip of the scratch probe. The *J*-integral was applied to evaluate the energy release rate from the perspective of an observer tied to the tip of the propagating crack; the following equation was then derived [7,8]:

$$F_T = K_c\sqrt{2pA_{LB}} \qquad (1)$$

where p is the perimeter, A_{LB} is the projected load-bearing contact area, and $2pA_{LB}$ is the probe shape function, which is calibrated using a reference material prior to testing [9]. In particular, for a spherical probe of radius R and for a penetration depth d, we have: $A_{LB} = \frac{2}{3R}(2Rd)^{3/2}$ and $p = \sqrt{2Rd}\beta\left(\frac{d}{R}\right)$ where $\lim_{x\to 0}\beta(x) = 1$. We employ dimensional analysis to derive the expression of the horizontal force:

$$F_T^2 = 2pA_{LB}\frac{K_c^2}{\mathcal{F}\left(\frac{l_{ch}}{\frac{A_{LB}}{2p}}, \frac{l_{ch}}{R}, \frac{H}{M}\right)} \qquad (2)$$

M is the material indentation modulus, H is the material indentation hardness, and $l_{ch} = \frac{K_c^2}{H^2}$ is the material characteristic length.

We define the nominal strength as: $\sigma_N = \frac{F_T}{A_{LB}}$

and we define the nominal size as $D = \frac{A_{LB}}{2p}$. For instance, for a test with a spherical probe, $D = \frac{\frac{2}{3}d}{\beta(d/R)}$. Thus, as the penetration depth d increases, the nominal size D increases also. The nominal strength σ_N and the nominal size D are then related by:

$$\sigma_N = \frac{K_c}{\sqrt{D\mathcal{F}\left(\frac{l_{ch}}{D}, \frac{l_{ch}}{R}, \frac{H}{M}\right)}} \qquad (3)$$

For a test on a given material with a given spherical probe, the second and third arguments are constant during the test, thus we can write:

$$\sigma_N = \frac{K_c}{\sqrt{D\tilde{\mathcal{F}}\left(\frac{l_{ch}}{D}\right)}} \qquad (4)$$

Where the functional $\tilde{\mathcal{F}}$ is specific to both the scratch probe and the material to test. For large penetration depths, the quantity $\frac{l_{ch}}{D}$ becomes very small and a first order Taylor expansion of functional $\tilde{\mathcal{F}}$ around the origin can be conducted: $\tilde{\mathcal{F}}(x) = \tilde{\mathcal{F}}(0) + \tilde{\mathcal{F}}'(0)x + o(x)$. By replacing $\tilde{\mathcal{F}}$ by its first-order Taylor expansion, we then derive the size effect law for scratch tests: $\sigma_N = \frac{K_c}{\sqrt{D\tilde{\mathcal{F}}(0) + \tilde{\mathcal{F}}'(0)\, l_{ch}}}$, that can be rewritten as:

$$\sigma_N = \frac{Bf_t'}{\sqrt{1 + D/D_0}} \qquad (5)$$

With $Bf_t' = \frac{K_c}{\sqrt{\tilde{\mathcal{F}}'(0)\, l_{ch}}}$ and $D_0 = \frac{\tilde{\mathcal{F}}'(0)\, l_{ch}}{\tilde{\mathcal{F}}(0)}$. Bf_t' and D_0 are SEL parameters and they are specific to both the scratch probe and the material to test.

Given experimental data $(\sigma_{N_i})_{1 \le i \le n}$ and $(D_i)_{1 \le i \le n}$ corresponding to a single progressive-load scratch test, the SEL parameters can be computed using a constrained optimization scheme. To this end, we define M and N that minimize the quantity:

$$\min \sum_i \left(y_i - \ln\left(\frac{M}{\sqrt{N + e^{x_i}}} \right) \right)^2 \qquad (6)$$

with $y_i = \ln \sigma_{N_i}$ and $x_i = \ln D_i$, where $\ln(x)$ denotes the natural logarithm function. The SEL parameters and the fracture toughness are then related to M and N via:

$$D_0 = N, Bf_t' = M\sqrt{N}, K_c = M \qquad (7)$$

Thus, we have a rigorous method to apply the size effect law to scratch test data and extract the fracture characteristics while accounting for a nonlinear fracture behavior.

5 RESULTS

Figs. 4 a) and b) display the recorded horizontal force and penetration depth curves for scratch tests on both unaltered and altered Mt Simon sandstone. Figs 4 c) and d) shows optical microscopic images of the residual

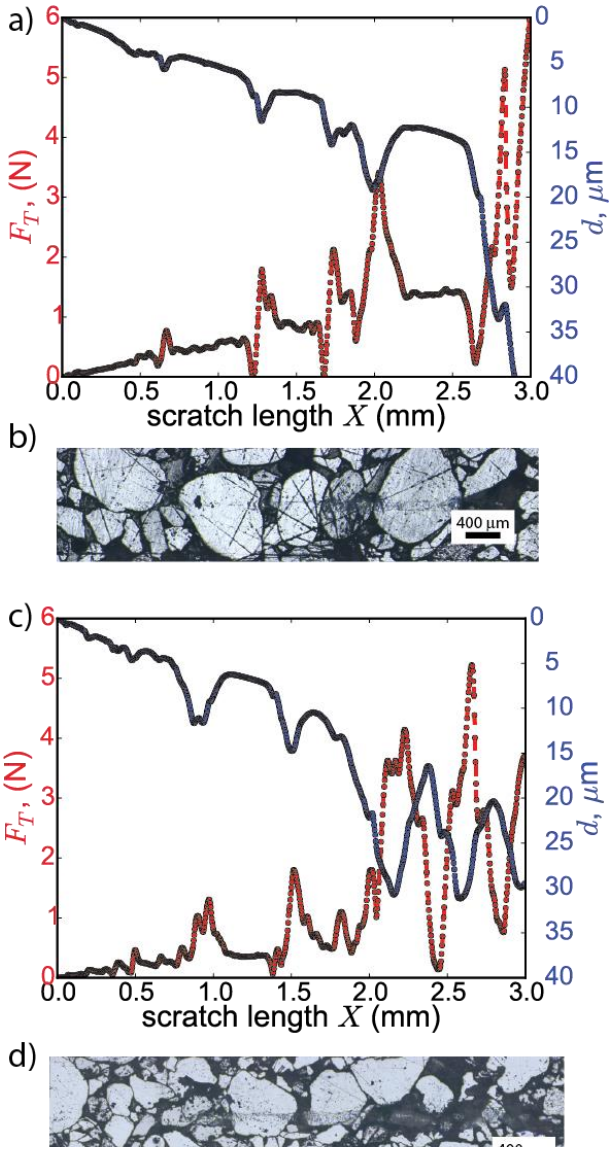

Figure 4: a)–b) Scratch test on unaltered Mt Simon sandstone. Force and depth curves and panorama of residual surface. c)–d) Scratch test on altered Mt Simon sandstone following incubation in CO_2-sturated brine. Force and depth curve and panorama of residual surface. F_T is the horizontal force, X is the scratch path, and d is the penetration depth.

surface after scratch testing.

During each test, as the vertical force is linearly increased, the horizontal force F_T increases as well, and so does the penetration depth d. Both the horizontal force and the penetration depth exhibit a saw-tooth evolution due to changes in composition and morphology occurring throughout the scratch path. Moreover, deep increases in penetration depth are preceded by a sudden increase in vertical force, which is a feature characteristic of sudden energy releases during microchipping processes [10]. The recorded maximum horizontal forces were in the range 5–6 N and the maximum penetration depths were in the range 30–50 µm. In our analysis, we focused on data points in the spherical range of the probe, with a penetration depth less than 27 µm.

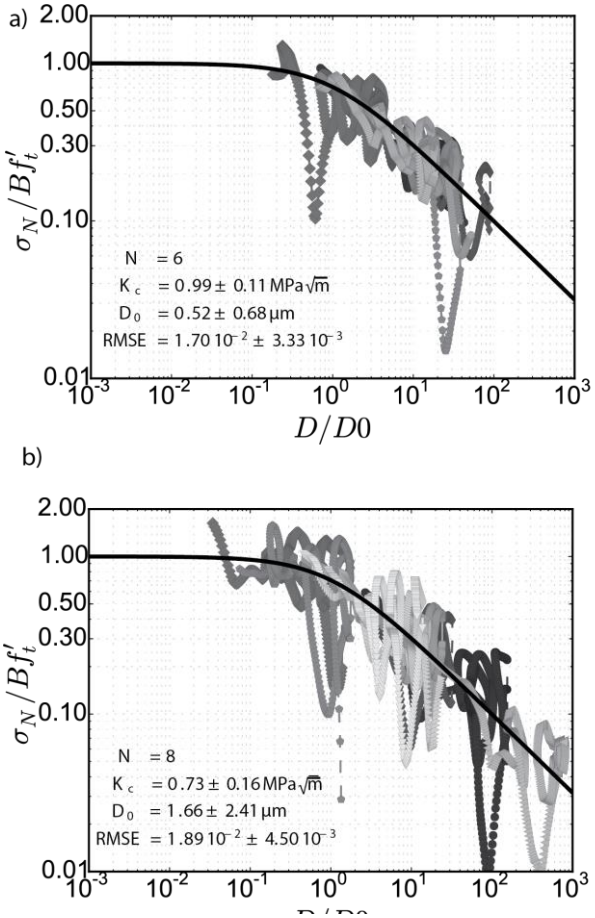

Figure 5: Size effect law applied to scratch tests on Mt Simon Sandstone**.** a) Unaltered Mt Simon sandstone. b) Altered Mt Simon sandstone. N is the number of tests, K_c is the fracture toughness, Bf_t' and D_0 are the SEL parameters, σ_N is the nominal strength, D is the nominal size, and $RMSE$ is the root mean squared error.

Fig. 5 displays the application of the size effect law to scratch tests on Mt Simon sandstone in the unaltered (Fig. 5 a)) and altered (Fig. 5 b)) states. A dimensionless representation of the size effect law is adopted with the x-variable being the dimensionless nominal size, D/D_0, and the y-variable being the dimensionless nominal strength, σ_N/Bf_t'. $N = 6$ scratch tests were carried out for unaltered Mt Simon sandstone whereas $N = 8$ tests were conducted on the incubated Mt Simon sandstone sample.

A good agreement is observed between theory and experiments as evidenced by the low values of the root mean squared error, $RMSE$. For the unaltered specimen, $RMSE = 1.70\ 10^{-2} \pm 3.33\ 10^{-3}$ whereas for the altered specimen, $RMSE = 1.89\ 10^{02} \pm 4.50\ 10^{-3}$.

A ductile-to-brittle transition is observed, which is driven by D and hence by the penetration depth d. The fracture behavior is nonlinear with the brittleness number $\lambda = D/D_0$ ranging between 1 and 10. The nonlinear fracture behavior points to a coexistence of ductile behavior and fracture during testing and justifies the use of the Size Effect Law to capture the transition from the strength asymptote to the Linear Elastic Fracture Mechanics asymptote.

A decrease in fracture toughness is observed for Mt Simon sandstone following incubation in CO_2-saturated brine. For the unaltered Mt Simon sandstone specimen, the fracture toughness was computed as $K_c = 0.99 \pm 0.11$ MPa$\sqrt{\text{m}}$ whereas for the altered Mt Simon sandstone specimen, the computed fracture toughness was $K_c = 0.73 \pm 0.16$ MPa$\sqrt{\text{m}}$. Thus, a 26% decrease in fracture toughness is observed following incubation in CO_2-saturated brine for 7 days under a pressure of 2500 psi (17.24 MPa) and at a temperature of 50°C.

The decrease in fracture toughness is accompanied by an increase in SEL characteristic length. For the unaltered Mt Simon sandstone specimen, the computed SEL characteristic length was $D_0 = 0.52 \pm 0.68$ µm and for the altered Mt Simon sandstone specimen, the computed characteristic length was $D_0 = 1.66 \pm 2.41$ µm. Based on Eq. (5),

the SEL characteristic length D_0 is a function of both the scratch probe —which was the same for all tests conducted in this study— and of the material elasto-plastic characteristics. Thus, the recorded 219% increase in SEL characteristic length suggests an increase in fracture process zone following incubation in CO_2-saturated brine under geological storage conditions.

7 DISCUSSION

We seek to relate the observed changes in fracture behavior to chemical and microstructural alterations caused by the incubation of Mt Simon sandstone in CO_2-saturated brine. To this end, we employ ion chromatography analyses, environmental scanning electron imaging and digital image analysis via machine learning statistical techniques.

7.1 CO_2-Induced Changes in Chemical Composition

Ion chromatography analysis was conducted to monitor changes in brine chemical composition following incubation of Mt Simon sandstone in CO_2-saturated brine.

Table 2: Ion chromatography analyses results. Concentration of the cations/anions in the brine before/after incubation with CO_2.

	Before incubation(mg/L)	After incubation(mg/L)	Change (%)
Li	1231.75	1222.58	-0.74
Na	44600.85	45550.37	2.13
K	1894.79	1981.41	4.57
Mg	2283.28	2339.46	2.46
Ca	19768.82	20122.59	1.79
Sr	873.06	871.43	-0.19

Our observations suggest the presence of CO_2-induced K-feldspar and clay dissolution reactions. Table 2 displays the changes in chemical concentrations for anions and cations before and after CO_2 alteration. A 4.57% increase in K is observed, which hints towards K-feldspar—$K(Si_3Al)O_8$— dissolution reactions. Similarly, the observed 2.46% increase in Mg concentration points towards clay dissolution reactions. The Si concentration is not affected suggesting a stability of quartz crystals during the incubation procedure.

These observations of geochemical dissolution reactions are supported by prior studies on the Mt Simon sandstone. Yoksoulian et al. [11] calculated mineral dissolution constants for the Mt Simon sandstone assuming incubation in CO_2-saturated brine under a pressure of 2030 psi (20.2 MPa) and a temperature of 50℃. The reported dissolution constants for respectively clay, K-feldspar, and quartz were: $k(\text{clay}) = 5.81 - 9.55\ 10^{-7}$ mole/m^2/s, $8.04\ 10^{-8}$ mole/m^2/s, and $3.8\ 10^{-12}$ mole/m^2/s. Consequently, clay and K-feldspar are more likely to dissolve compared the quartz whose dissolution constant in four orders of magnitude smaller.

7.2 CO_2-Induced Microstructural Changes

In order to study CO_2-induced microstructural changes, environmental backscattered secondary electron microscopy was conducted using a FEI Quanta 650 under low vacuum and with an accelerating voltage of 20 kV. Fig. 5 displays the corresponding micrographs for both unaltered Mt Simon sandstone (Fig. 5 a)) and altered Mt Simon sandstone (Fig. 5 b)) with a magnification level of 55×. K-feldspar grains can be seen in bright color and quartz grains are in dark gray. The area imaged is of the size 3.6 mm × 2.4 mm, with a size five times greater than the size of individual grains.

An increase in pore throat size is observed along with localized increases in porosity. In Fig. 5, the maximum pore throat size is shown

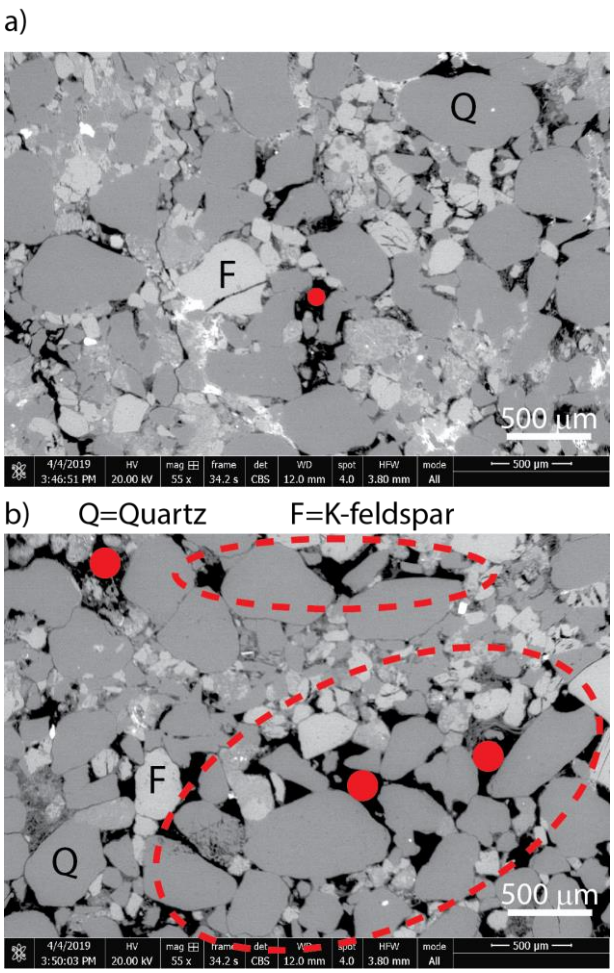

Figure 6: CO_2-induced microstructural changes in Mt Simon sandstone via backscattered secondary electron imaging. a) Unaltered Mt Simon sandstone specimen. b) Altered Mt Simon sandstone specimen**.** The red dots indicate the maximum pore throat sizes. The dotted red ellipses point to regions of localized porosity increase.

using red dots. For unaltered Mt Simon sandstone, the maximum pore throat size is 104 µm. For altered Mt Simon sandstone, the maximum pore throat size is 182 µm. Thus, incubation into CO_2-saturated brine results in a 75% increase in the pore throat size. Moreover, there are regions of localized increase in porosity that are shown in Fig 6 b) using dotted red ellipses. The increase in pore throat size and the non-uniform increase in porosity have been reported on other rock systems. Vialle et al. reported an increase in macropore size after flushing carbonate rock samples with CO_2-rich water [12]. Similarly, Rimmele et al. reported localized porosity gradients for Lavoux limestone exposed to CO_2-saturated water. These microstructural changes are usually

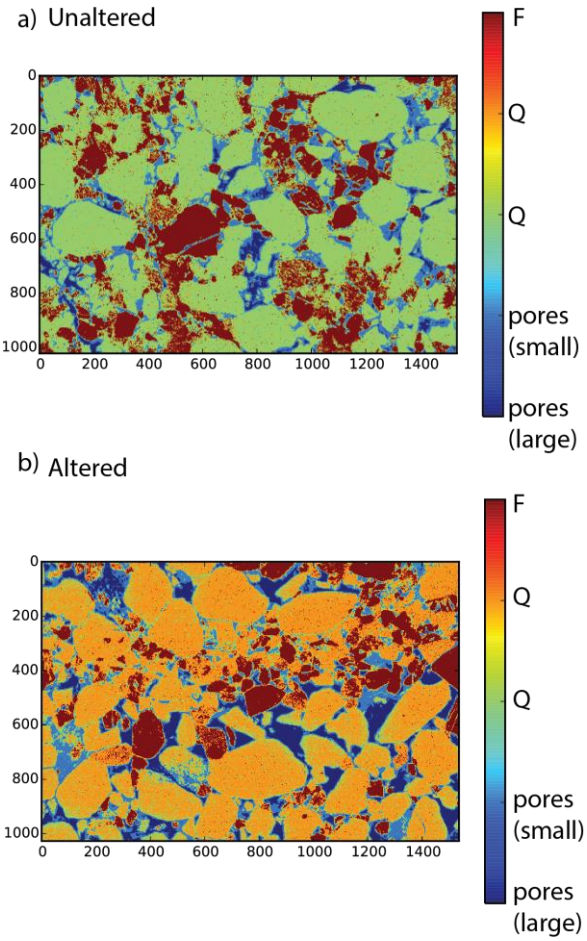

Figure 7: Phase identification on Mt Simon sandstone using machine learning-inspired Gaussian mixture modeling. F= K-feldspar, Q= quartz. a) Unaltered Mt Simon sandstone: 1,569792 pixels sampled. b) Altered Mt Simon sandstone: 1,579,008 pixels sampled.

Table 3: Estimated phase distribution based on Gaussian mixture modelling of back-scattered secondary electron micrographs for both altered and unaltered Mt Simon sandstone. F=K-feldspar. Q=quartz.

	Unaltered	Altered
F	25% vol	17% vol
Q	59% vol	60% vol
Q		
Pores (small)	16% vol	18 % vol
Pores (large)	2% vol	8% vol

attributed to underlying dissolution reactions.

In order to further investigate potential CO_2-induced chemical changes, we apply machine learning-inspired gaussian mixture modelling. The basic idea is capitalize on the spatially-resolved sampling of the gray levels. In backscattered secondary electron imaging, the gray level is reflective of the local elemental composition of the material. Therefore, minerals can be differentiated based on their gray levels: for instance, quartz grains are shown in dark gray, feldspar grains are shown in bright color and air voids are shown in black. One consequence is that if we sample the gray level distribution at each pixel and apply a Gaussian mixture model, we can then recover the chemical phase distribution over the area imaged.

Figure 7 illustrates our approach on both unaltered and altered Mt Simon sandstone. For each material, we imaged an area of size 3.6 mm × 2.4 mm while sampling over 1.5 million pixels. The identified chemical phases are represented. In addition, we can quantify their area fraction—which is assumed to be equal to their volume fraction for perfectly disordered materials. Table 3 reports the estimated volume fraction for K-feldspar, quartz, and micropores, both small and large.

We observe a decrease in K-feldspar and an increase in the fraction of large micropores. Thus, Gaussian mixture modelling of backscattered secondary electron micrographs provides further confirmation of CO_2-induced K-feldspar dissolution reactions.

8 CONCLUSIONS

Our research objective was to investigate the influence of CO_2-induced geochemical reactions on the fracture behavior of Mt Simon sandstone. To this end, we carried out microscopic scratch tests, ion chromatography tests, and environmental back-scattered secondary electron imaging on both unaltered and altered Mt Simon sandstone samples. The alteration was conducted in a flow-through experiment with CO_2-saturated brine at 2500 psi and 50℃ for 7 days. Our major findings are summarized below:

- Mt Simon sandstone exhibits a nonlinear fracture behavior and therefore, the Size Effect Law is important to measure the fracture parameters.
- CO_2-incubation results in a decrease in fracture toughness and an increase in the fracture process zone of Mt Simon sandstone. These mechanical changes are due to CO_2-induced microstructural and compositional changes.
- Microstructural changes are observed following incubation of Mt Simon sandstone in CO_2-saturated brine, notably: an increase in pore throat size, an overall increase in the fraction of large pores, and localized porosity gradients.
- Evidence of geochemical reactions was observed: K-feldspar dissolution and potentially clay dissolution.

Thus, scratch tests provide a viable tool to investigate geo-chemo-mechanical alterations during geological carbon sequestration.

ACKNOWLEDGMENTS

This work was supported as part of the Center for Geologic Storage of CO2, an Energy Frontier Research Center funded by the U.S. Department of Energy, Office of Science, Basic Energy Sciences under Award # DE-SC0C12504. The authors would like to thank the Illinois State Geological Survey for providing the Mt. Simon sandstone specimens tested and analyzed in this investigation. This work made use of the EPIC facility of Northwestern University's NU*ANCE* Center, which has received support from the Soft and Hybrid Nanotechnology Experimental (SHyNE) Resource (NSF ECCS-1542205); the MRSEC program (NSF DMR-1720139) at the Materials Research Center; the International Institute for Nanotechnology (IIN); the Keck Foundation; and the State of Illinois, through the IIN.

REFERENCES

[1] Will, R., El-Kaseeh, G., Jaques, P., Greenberg, S., Finley, R., 2016a. Microseismic data acquisition, processing,

and event characterization at the Illinois Basin - Decatur Project. *Int. J. Greenh. Gas Control* **54**, 404–420.

[2] Bauer, R.A., Carney, M., Finley, R.J., 2016a. Overview of microseismic response to CO_2 injection into the Mt. Simon saline reservoir at the Illinois Basin-Decatur Project. *Int. J. Greenh. Gas Control* **54**, 378–388.

[3] Tudek, J., Crandall, D., Fuchs, S., Werth, C.J., Valocchi, A.J., Chen, Y. and Goodman, A., 2017. In situ contact angle measurements of liquid CO_2, brine, and Mount Simon sandstone core using micro X-ray CT imaging, sessile drop, and Lattice Boltzmann modeling. *Journ. Petr. Sci. Eng.*, **155**, 3-10.

[4] Sun, Z., Espinoza, D.N., Balhoff, M.T. and Dewers, T.A., 2017. Discrete Element Modeling of Micro-scratch Tests: Investigation of Mechanisms of CO 2 Alteration in Reservoir Rocks. *Rock Mech. & Rock Eng.*, *50*(12), pp.3337-3348.

[5] Sun, Y., Aman, M. and Espinoza, D.N., 2016. Assessment of mechanical rock alteration caused by CO2 water mixtures using indentation and scratch experiments. *Int. J. Greenh. Gas Control*, *45*, pp.9-17.

[6] Major, J.R., Eichhubl, P., Dewers, T.A., Urquhart, A.S., Olson, J.E. and Holder, J., 2014, August. The effect of CO 2-related diagenesis on geomechanical failure parameters: fracture testing of CO 2-altered reservoir and seal rocks from a natural analog at Crystal Geyser, Utah. In *48th US rock mechanics/geomechanics symposium*. American Rock Mechanics Association.

[7] Akono, A.T. and Ulm, F.J., 2012. Fracture scaling relations for scratch tests of axisymmetric shape. *J. Mech. and Phys. Sol.*, **60** (3), pp.379-390.

[8] Akono, A.T., Randall, N.X. and Ulm, F.J., 2012. Experimental determination of the fracture toughness via microscratch tests: Application to polymers, ceramics, and metals. *J. Mat. Res.*, **27**(2), pp.485-493.

[9] Akono, A.T. and Ulm, F.J., 2014. An improved technique for characterizing the fracture toughness via scratch test experiments. *Wear*, **313**(1-2), pp.117-124.

[10] Atkins, T., 2009. *The Science and Engineering of Cutting*. Butterworth-Heinemann.

[11] Yoksoulian, L.E., Freiburg, J.T., Butler, S.K., Berger, P.M. and Roy, W.R., 2013. Mineralogical alterations during laboratory-scale carbon sequestration experiments for the Illinois Basin. *Energy Procedia*, **37**, 5601-5611.

[12] Vialle, S. and Vanorio, T., 2011. Laboratory measurements of elastic properties of carbonate rocks during injection of reactive CO2-saturated water. *Geoph. Res. Lett.*, **38**(1).